# Catalysis Science & Technology

Accepted Manuscript






ROYAL SOCIETY OF CHEMISTRY

www.rsc.org/catalysis

 Journal Name Catalysis Science & Technology Dynamic Article Links ►

Cite this: DOI: 10.1039/c0xx00000x

www.rsc.org/xxxxxx

ARTICLE TYPE

# Direct Amination of Benzene to Aniline with $H_2O_2$ and $NH_3 \cdot H_2O$ over $Cu/SiO_2$ Catalyst†

**Tianhua Yu[a,b], Ruiguang Yang[a], Sheng Xia[a], Guiying Li[a,*], Changwei Hu [a,*]**

***Received (in XXX, XXX) Xth XXXXXXXXX 20XX, Accepted Xth XXXXXXXXX 20XX***

**DOI: 10.1039/b000000x**

## Graphical abstract

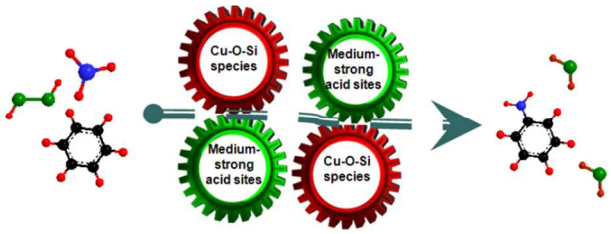


Cu/S-1 catalyst activated the N-H bond of $NH_3$ and C-H bond of benzene, leading to the formation of aniline.

Cite this: DOI: 10.1039/c0xx00000x

www.rsc.org/xxxxxx

ARTICLE TYPE

# Direct Amination of Benzene to Aniline with $H_2O_2$ and $NH_3 \cdot H_2O$ over $Cu/SiO_2$ Catalyst†

**Tianhua Yu[a,b], Ruiguang Yang[a], Sheng Xia[a], Guiying Li[a,*], Changwei Hu [a,*]**

***Received (in XXX, XXX) Xth XXXXXXXXX 20XX, Accepted Xth XXXXXXXXX 20XX***

**DOI: 10.1039/b000000x**

The direct amination of benzene to aniline with $H_2O_2$ and $NH_3 \cdot H_2O$ was studied over a series of $Cu/SiO_2$ catalysts with mesoporous structure under mild conditions, and acceptable yield (5.4%) and selectivity (74.0%) to aniline were obtained. Ultraviolet-visible diffuse reflectance spectroscopy, Fourier transform infrared spectroscopy and X-ray photoelectron spectroscopy demonstrated that part of Cu atoms incorporated into the mesoporous silica network forming Cu-O-Si species, which could promise the selective activation of the N-H bond of $NH_3$. The medium-strong acid sites were beneficial to amination reaction. The concentration of the reactants was found to be another critical factor for aniline formation. The aromatic ring amination of substituted benzenes have been also investigated under the optimized conditions.

## 1. Introduction

Aniline is an important precursor or intermediate for the production of agrochemicals, dyes and pharmaceuticals.[1-3] Current commercial methods for the preparation of aniline involve multiple reaction steps with many disadvantages, such as the use of corrosive materials and complicated apparatus, the production of waste, and related environmental problems.[4-9] A very attractive and challenging method for the preparation of aniline directly from benzene was first reported by Wibaut in 1917, where aniline could be obtained by passing benzene and ammonia over a reduced iron/nickel catalyst at 550-600 ℃.[10] Later, many researchers tried to shift the reaction equilibrium towards aniline production by removing the hydrogen formed.[11-17] However, these methods still suffer from disadvantages on energy consumption, equipment costs and harsh reaction conditions. In 2013, Yoshida et al obtained aniline (0.066% yield) over a platinum loaded titanium oxide photocatalyst with $NH_3 \cdot H_2O$ under optimized conditions with emphasis on the reaction mechanism.[18] Our previous studies indicated that $H_2O_2$ was a desired oxidant for the direct synthesis of aniline from benzene with ammonia, although the yield of aniline was still not satisfactory.[19-21] The direct, one-step amination of benzene to aniline generally suffers from relatively low conversion of benzene and/or relatively low selectivity to aniline, so it has not been adopted in industry.[11,12] However, many researchers are still deeply attracted by this fantastic research field.

Cu-based catalysts are well known as efficient catalyst for various reactions, such as, hydrogenation process,[22-25] and activation of benzene halide and ammonia.[3,26,27] Moreover, copper oxide could be also used as reducible metal oxide in the direct amination from benzene to aniline.[16] Our previous work[20] showed that titanium-silicalite-1 (TS-1) catalyst displayed acceptable activity to the direct amination of benzene to aniline. The loading of copper species on TS-1 enhanced remarkably the activity of the catalysts and increased the yield of aniline to 1% under mild conditions. Recently, we found that the use of reactive distillation (RD) reactor could further promote the yield of aniline to 12.4% over hierarchical TS-1 (h-TS-1) supported copper catalyst.[19]

Though TS-1 and h-TS-1 are excellent supports for the direct amination of benzene to aniline, there exist some inherent problems in the preparation, such as difficult duplication, expensive cost and complex technology, which severely restrict their practical application. Finding a new support as alternative is a good way to overcome the above shortcomings. As a widely used support for many catalysts, silicalite-1 (S-1) with mesoporous structure possesses similar crystal and pore structure as well as surface area ($S_{BET}$) to TS-1 and h-TS-1. However, no study regarding the use of Cu/S-1 catalyst in the direct amination of benzene to aniline has been reported though the preparation of S-1 is relatively easier. This study aims to develop a new catalyst which could be produced simply, and get some new insights into the amination of benzene to aniline.

## 2. Experimental

### 2.1. Catalyst preparation

S-1 was synthesized basically according to the procedures reported the literature[28]. The details were given in supporting information (S1†).

For mesoporous silica (Meso-1) synthesis,[29] 2.4 g of cetyltrimethylammonium bromide and 120.0 g of $H_2O$ were mixed and stirred until the solution became clear. 8.0 ml of 28%

ammonia solution was added, followed by addition of 9.4 g of TEOS. After stirring for 24 h, the precipitate was filtered, dried at 100 ℃ overnight, and calcined at 550 ℃ for 6 h in air. As a reference support in the previous work[20], commercial porous silica from Qingdao Xinchanglai Silicone Limited Company was also used and denoted as Meso-2 in the present work.

$Cu/SiO_2$ catalyst was prepared by impregnation method. First, an aqueous solution of $Cu(NO_3)_2$ was dropped onto the $SiO_2$ support in a 50 ml beaker, and the slurry was stood for 24 h at room temperature. The excess $H_2O$ was removed by heating in a water bath at 80 ℃, and the resultant solid was dried overnight in vacuum at 110 ℃, and then calcined at 550 ℃ for 6 h in air. Finally, the catalysts were obtained and denoted as x wt% support (x the controlled Cu content).

### 2.2. Catalyst characterization

X-ray diffraction (XRD) measurements of the samples were performed on a LTD DX-1000 CSC diffractometer using Cu-Kα radiation (λ = 0.15406 Å) with a scanning angle (2θ) from 5 to 75 °. The tube voltage was 40 kV and the current was 30 mA.

$N_2$ adsorption-desorption isotherms were measured by static $N_2$ physisorption at -196 °C with a Micromeritics Tristar 3020 $S_{BET}$ and pore analyser. Prior to $N_2$ adsorption-desorption, the samples were degassed at 100 °C for 1 h and then evacuated at 300 °C for 4 h to remove physically adsorbed impurities. $S_{BET}$ was calculated by Brunauer-Emmett-Teller (BET) method. The total pore volume ($V_p$) was derived from the adsorbed $N_2$ volume at a relative pressure of approximately 0.99, and the Barrett-Joyner-Halenda method was used to calculate the pore size distributions according to the desorption branches of isotherms.

Ultraviolet-visible diffuse reflectance (DR UV–vis) spectra were obtained in the range from 200 to 800 nm using a TU-1901 spectrometer equipped with a reflectance attachment. $BaSO_4$ was used as the reference material.

Fourier transform infrared (FT-IR) spectra were collected at 2 $cm^{-1}$ resolution on a Nicolet Nexus 670 FT-IR spectrometer equipped with a mercury cadmium telluride detector. The powder samples were mixed with KBr (1 wt%) and pressed into translucent disks at room temperature.

Transmission electron microscopy (TEM) images were obtained on a FEI company Tecnai $G2^{20}$ Stwin instrument operated at 200 kV. The samples were ultrasonically dispersed in ethanol at room temperature for 6 h. The as-obtained solution was dropped onto the copper grids for TEM.

X-ray photoelectron spectroscopy (XPS) was measured on an AXIS Ultra DLD (KRATOS) spectrometer with Al-Kα radiation. The obtained binding energy (BE) was calibrated using the C 1s peak at 284.8 eV as the reference, and a Shirley background was subtracted from all spectra. Then peak fitting was performed using an 80/20 Lorentz-Gauss function.

The samples were also characterized by $NH_3$ temperature programmed desorption ($NH_3$-TPD). A multichannel HP R-20QIC mass spectrometry was also used to analyze the released gases ($NH_3$-TPD-MS). 0.20 g of sample in a stainless steel U-tube was flushed in $N_2$ at 300 ℃ for 1 h. After cooling to 60 ℃, the gas was switched to pure $NH_3$ with a flow rate of 30 ml $min^{-1}$ for 25 minutes. Weakly adsorbed $NH_3$ was removed by pure He sweeping at 60 ℃ until the baseline of Thermal Conductivity Detector and MS signals stabilized. Under an atmosphere of purified He with a flow rate of 30 ml $min^{-1}$, $NH_3$-TPD was conducted from 60 to 800 ℃ at a ramping of 10 ℃ $min^{-1}$. The possible molecules ($N_2O$, NO, $NO_2$, and $NH_3$) from desorption or reactive desorption of $NH_3$ were monitored with MS signals of $m/e$ = 44, 30, 46 and 17.

The chemical analysis of the samples was performed by using the inductively coupled plasma (ICP) technique to measure the Cu loading (thermo E.IRIS).

### 2.3. Measurements of catalytic activity

Direct amination of benzene was performed in a 50 ml single neck flask equipped with a reflux condenser and a stirrer in a sealed system. Typically, 0.5 g 2.5 wt% Cu/S-1 and 2.8 mmol benzene were loaded into the flask. The reaction was carried out with stirring when the temperature of the reactor reached 60 ℃. A mixture consisted of 40.0 ml $H_2O$, 133.0 mmol $NH_3 \cdot H_2O$ and 18.1 mmol $H_2O_2$ was prepared and kept at 0 ℃. The mixture was fed into the reaction system with the velocity of 0.2 ml $min^{-1}$ from the top of the condenser by peristaltic pump. After the addition of the mixture was completed, the reaction was carried out for another 0.5 h under the same reaction conditions. Then, the reaction system was cooled down to room temperature.

The analysis of the products and related calculation methods were the same as those in the previous report (S2†).[19]

## 3. Results and Discussion

### 3.1. Catalyst characterisation

#### 3.1.1 XRD

Fig. 1A shows the XRD patterns of the three bare supports and fresh samples containing 2.5 wt% copper. For Meso-1 and Meso-2, no obvious diffraction peaks could be observed, indicating that Meso-1 and Meso-2 presented in amorphous state.[30] The diffraction peaks of S-1 were coincident with the mobil five (MFI) zeolitic topology with a monoclinic symmetry (signals at 2θ ranged 7-9°, 23-25° and 45°).[31] In addition, no diffraction peaks from cupric oxide or any related cupreous substances could be detected in the three samples containing 2.5 wt% copper, suggesting that copper species were highly dispersed on the three supports.

XRD patterns of the samples with different Cu loading on S-1 are shown in Fig. 1B. When Cu loading was greater than 5.5 wt%, two diffraction peaks at 2θ of 36.5° and 38.8° characteristic of CuO were observed, and their intensity increased with the increase of Cu loading, implying that copper oxide aggregated into large particles.[32]

For the used samples containing 2.5 wt% copper (Fig. S1†), the peak positions were not changed, which showed that the structure of the samples remained after being used.

#### 3.1.2 $N_2$ adsorption-desorption isotherm

$N_2$ adsorption-desorption isotherms and pore size distributions of the samples are shown in Figs. S2-4†. According to the International Union of Pure and Applied Chemistry classification[33], all the isotherms exhibited characteristic type IV curves with capillary condensation that signified the presence of mesopores. $S_{BET}$ and pore structure parameters of all the samples are summarized in Table 1. The average pore diameters of all

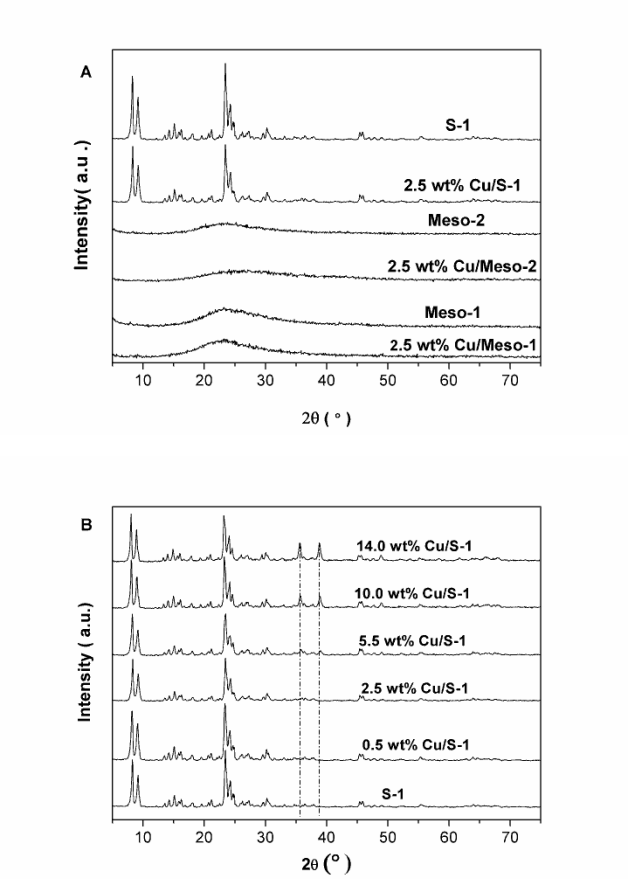


**Fig. 1.** XRD patterns of the samples: (A) the bare supports and fresh 2.5 wt% Cu loading samples. (B) the fresh catalysts with different Cu loading on S-1 samples.

the samples resided in the range of 25.9-81.0 Å, confirming that all the samples possessed mesoporous structure. Among the three bare supports, $S_{BET}$ followed the order: Meso-1 > Meso-2 > S-1. It was also found that the loading of copper on the bare supports obviously decreased the $S_{BET}$ and $V_p$. For the samples containing 2.5 wt% copper, the decrease of $S_{BET}$ and $V_p$ were 44% and 21% for Cu/Meso-1, 23% and 14% for Cu/Meso-2, only 8% and 5% for Cu/S-1, respectively. It was likely that the porous space inside the support was occupied and the smaller pore mouth was blocked by copper oxide introduced. As shown in Fig. S2†, the pore size distributions became broader after Cu loaded.[34] For the fresh Cu/S-1, the $S_{BET}$ and $V_p$ gradually decreased with the increase of Cu loading from 0.5 to 14.0 wt%. It seemed that more porous space inside the support was occupied and the larger pore mouth was blocked with increasing amount of copper oxide introduced.

For the used samples, the loss of $S_{BET}$ was more drastic for Cu/Meso-1 and Cu/Meso-2 than that for Cu/S-1; especially, on the used 2.5 wt% Cu/Meso-1, $S_{BET}$ decreased by 68%. The decrease in $S_{BET}$ may be attributed to partial collapse of the mesoporous network, caused by the vigorous stirring condition and liquid-phase nature of the reaction.[35] Because the structure of S-1 possessed strong stability, the $S_{BET}$ loss of Cu/S-1 was small after being used.

**Table 1.** The textural properties and chemical compositions of the catalysts.

| Sample | $S_{BET}$ ($m^2$ $g^{-1}$) | $V_P$($cm^3$ $g^{-1}$) | $\Phi_P$(Å)[b] | Cu (wt%)[c] | Cu (wt%)[d] |
|---|---|---|---|---|---|
| S-1 | 420 | 0.43 | 41.3 | - | - |
| Meso-1 | 889 | 0.58 | 25.9 | - | - |
| Meso-2 | 478 | 0.96 | 81.0 | - | - |
| 0.5Cu/S-1[a] | 400 | 0.42 | 41.8 | 0.49 | 0.12 |
| 2.5Cu/S-1 | 387 | 0.41 | 57.0 | 2.48 | 0.33 |
| 5.5Cu/S-1 | 375 | 0.41 | 44.5 | 5.47 | 0.52 |
| 10.0Cu/S-1 | 368 | 0.38 | 41.6 | 9.95 | 0.80 |
| 14.0Cu/S-1 | 339 | 0.35 | 41.6 | 13.92 | 0.88 |
| 2.5Cu/S-1(used) | 341 | 0.47 | 55.7 | 2.28 | 0.30 |
| 2.5Cu/Meso-1 | 500 | 0.46 | 36.8 | 2.47 | 1.98 |
| 2.5Cu/Meso-1(used) | 281 | 0.45 | 63.8 | 1.73 | 1.39 |
| 2.5Cu/Meso-2 | 390 | 0.83 | 84.9 | 2.48 | 5.77 |
| 2.5Cu/Meso-2(used ) | 324 | 0.91 | 88.2 | 1.87 | 0.60 |

[a] 0.5 wt% Cu/S-1 was abbreviated to 0.5Cu/S-1 and other samples were also abbreviated analogously. [b] Adsorption average pore width. [c] Total Cu loading determined by ICP. [d] Surface Cu loading determined by XPS.

### 3.1.3 DR UV–vis and FT-IR spectroscopy

In the literature,[36,37] the 600–800, 440 and 230 nm DR UV-vis bands were assigned to the d-d transition of Cu (II) ions in the octahedral ligand field generated by the oxygen ions, the charge-transfer (CT) of $O_{bridge}$→Cu transition in the $Cu_2O_2$ moiety and CT of O→Cu transitions of isolated Cu (II) ions in coordination with lattice oxygen, respectively. Fig. 2A shows the spectra of the three bare supports and fresh samples containing 2.5 wt% copper. For the three bare supports, no peaks were observed over the examined wavelength range of 200-800 nm. After copper species was introduced (Figs. 2A and S5†), the spectra were characterized by a d-d band in the region of 600–800 nm and an intense CT band at 230 nm. For the 2.5 wt% Cu/Meso-2, an obvious peak at about 440 nm was observed, and $S_{230}$ / $S_{440}$ / $S_{600\text{-}800}$ (the ratio of the peak area at 230 nm to the peak area at 440 nm to the peak area 600-800 nm) was 1.0 / 0.9 / 0.9. However, no band at about 440 nm was detected over 2.5 wt% Cu/Meso-1 and Cu/S-1, and $S_{230}$ / $S_{600\text{-}800}$ was 1.0 / 0.4 and 1.0 / 1.2, respectively. These results indicated that Cu-O-Si species was formed in all the samples containing copper. Cu-O-Si species was liable to be generated over Meso-1 support. However, the formation of Cu-O-Cu species was easier on Cu/Meso-2.

For the fresh Cu/S-1 (Figs. 2B and S5†), as the Cu loading increased from 0.5 to 4.0 wt%, $S_{230}$ / $S_{600\text{-}800}$ went up initially, reached the maximum of 1.0 / 1.2 at 2.5 wt%, and then decreased to 1.0 /3.0. When the Cu loading was greater than 5.5 wt%, the band at about 440 nm appeared, and $S_{230}$ / $S_{440}$ / $S_{600\text{-}800}$ varied from 1.0 / 0.8 / 3.0 to 1.0 / 3.0 / 6.0 with the increase of Cu loading to 14.0 wt%. The results revealed that the doped copper atoms incorporated mainly into the mesoporous silica oxide network at low Cu loading, and generated dispersed CuO species after the Cu loading reached 2.5 wt%, and then formed Cu-O-Cu species with higher Cu loading. The amount of Cu-O-Cu species increased obviously with the increase of Cu loading and that of Cu-O-Si species decreased dramatically with the increase of Cu-O-Cu species.

Fig. 3 shows the FT-IR spectra of the samples. For the three bare supports (Fig. 3A), both the bands at 3430–3450 and 1630–

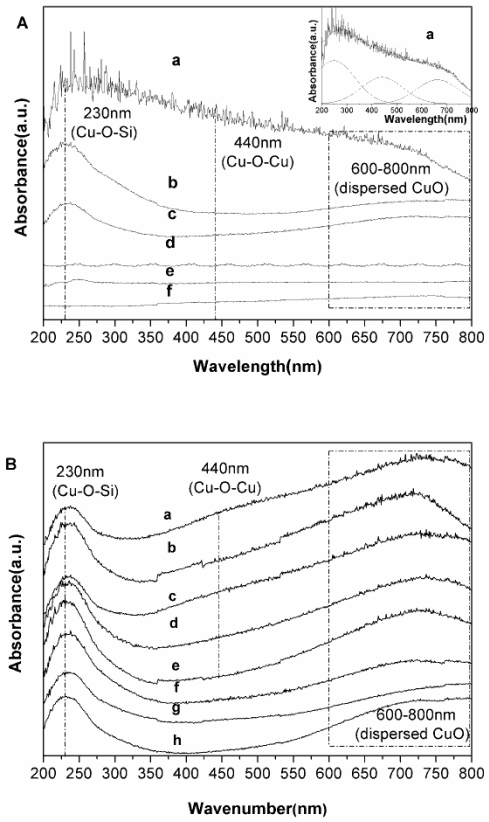


**Fig. 2.** DR UV–vis spectra of the samples: (A) a 2.5 wt% Cu/Meso-2; b 2.5 wt% Cu/Meso-1; c 2.5 wt% Cu/S-1; d Meso-2; e Meso-1; f S-1. (B) a 14.0 wt% Cu/S-1; b 10.0 wt% Cu/S-1; c 7.0 wt% Cu/S-1; d 5.5 wt% Cu/S-1; e 4.0 wt% Cu/S-1; f 2.5 wt% Cu/S-1; g 1.0 wt% Cu/S-1; h 0.5 wt% Cu/S-1.

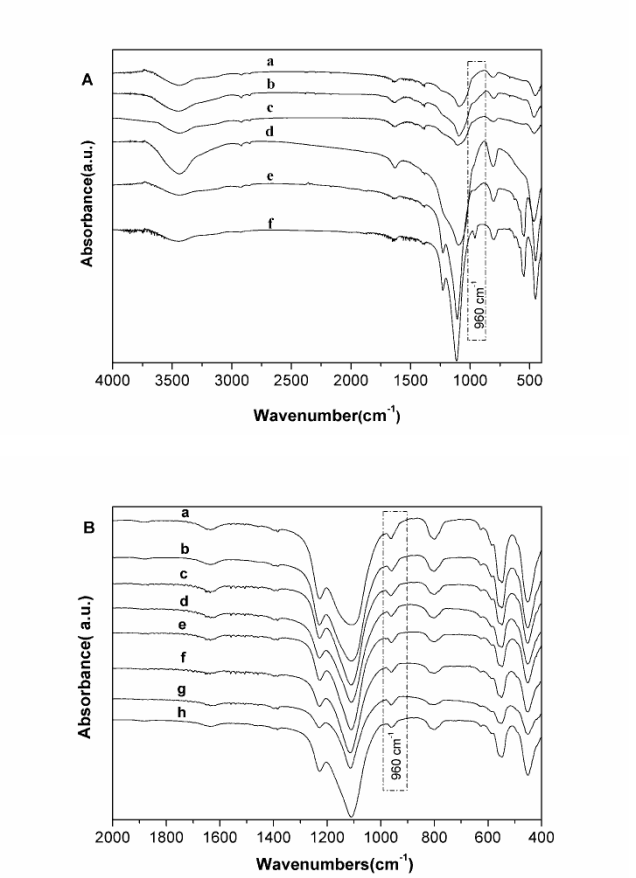


**Fig. 3.** FT-IR spectra of the samples: (A) a Meso-1; b 2.5 wt% Cu/Meso-1; c Meso-2; d 2.5 wt% Cu/Meso-2; e S-1; f 2.5 wt% Cu/S-1. (B) a 14.0 wt% S-1; b 10.0 wt% Cu/S-1; c 7.0 wt% Cu/S-1; d 5.5 wt% Cu/S-1; e 4.0 wt% Cu/S-1; f 2.5 wt% Cu/S-1; g 1.0 wt% Cu/S-1; h 0.5 wt% Cu/S-1.

1640 $cm^{-1}$ were attributed to the stretching vibration and the bending vibration of O-H bond in physisorbed $H_2O$, respectively, indicating the hydrophilic character of $SiO_2$.[38] The band at 470 $cm^{-1}$ was assigned to the Si-O-Si bending vibration, while the bands at 800–816 and 1090–1115 $cm^{-1}$ were caused by Si-O-Si symmetric stretching vibration and the Si-O-Si asymmetry stretching vibration, respectively.[38,39] For the S-1, a band near 550 $cm^{-1}$ was observed which was due to the stretching vibration of structural double five-member rings.[40] Thus the appearance of this band gave evidence that S-1 support possessed an atomic ordering of the MFI structure. These results agreed well with the XRD measurements. Compared to the three bare supports, these bands still preserved and actually unchanged after copper was introduced. For the Cu/S-1 (Fig. 3B), a band centred at 960 $cm^{-1}$, ascribed to the formation of Cu-O-Si hetero-linkage, testified the successful incorporation of copper into the silica framework,[41] which accorded with the DR UV–vis measurements. However, no absorbance at 960 $cm^{-1}$ was clearly detected from the spectra of Cu/Meso-1and Cu/Meso-2, which was probably due to the overlap of the band from the Si-O-Si asymmetry stretching vibration.[38]

### 3.1.4 TEM

TEM images in Fig. S6† show that 2.5 wt% Cu/S-1 possessed well crystalline monoclinic particles with an average diameter of approximately 100-150 nm (Fig. S6a and b†), indicating that the prepared S-1 had the MFI crystal structure.[42] However, 2.5 wt% Cu/Meso-1 and Cu/Meso-2 had an irregular mesostructure with sponge like mesoporous morphologies (Fig. S6d, e, g and h†),[43] and the pore size of Meso-2 was larger than that of Meso-1. There was no detectable agglomeration of copper species condensed on the supports, suggesting that the metallic particles were dispersed uniformly. The high dispersion could be associated with the relatively larger $S_{BET}$ of the supports that provided favourable dispersing effect for the copper species.

For the used samples (Fig. S6c, f and i†), the characteristics of crystalline of Cu/S-1 were unchanged, but the structures of Cu/Meso-1 and Cu/Meso-2 were severely destroyed in the reaction. The results conformed to the BET measurements and showed that Cu/S-1 was the most stable in surface and pore structure among the three samples.

### 3.1.5 XPS

The XPS profiles (Cu 2p) of the samples are reported in Fig. 4. The intense and broad photoelectron peak at about 934.0 eV (Cu $2p_{3/2}$) observed for the three Cu-based samples were in agreement with literature[44] concerning the copper oxide systems supported on different oxidic phases.

Fig. 4 shows that copper existed in the oxidation state of $Cu^{2+}$



 

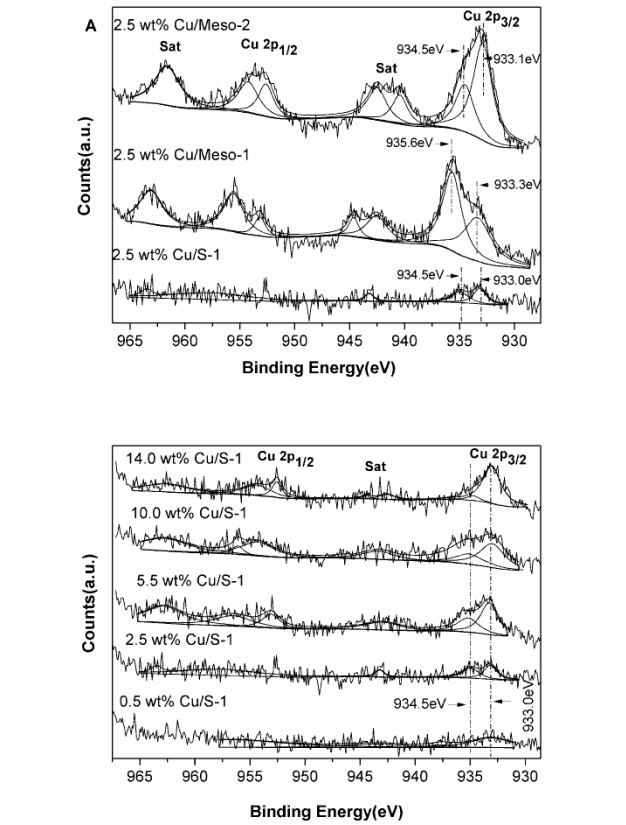


**Fig. 4.** XPS of the samples: (A) the fresh 2.5 wt% Cu loading samples. (B) the fresh catalysts with different Cu loading on S-1 samples.

on all the samples, evidenced by the Cu $2p_{3/2}$ peak at 932.8-935.6 eV and the 2p→3d satellite at 942.0-944.0 eV characteristic of $Cu^{2+}$ with electron configuration of $d^9$.[45] As shown in Fig. 4A, the XPS profiles of the three samples containing 2.5 wt% copper presented two contributions to the Cu $2p_{3/2}$ peaks, that is, 933.0 and 934.5 eV for Cu/S-1; 933.3 and 935.6 eV for Cu/Meso-1; 933.1 and 934.5 eV for Cu/Meso-2, respectively, indicating that two kinds of Cu (II) species with different microenvironments existed on these samples.[46] Typically, dispersed CuO species was observed at about 933.0 eV, and the shift to higher BE was indicative of a CT from the metal ion toward the support oxide, suggesting the formation of Cu-O-Si species.[45]

As shown in Table 1, the mass concentration ratios of the surface Cu content ($c_{S,Cu}$) obtained from XPS to the total Cu content ($c_{T,Cu}$) obtained from ICP, were calculated to be the values 0.13 for Cu/S-1, 0.80 for Cu/Meso-1 and 2.32 for Cu/Meso-2, when the samples contained 2.5 wt% copper. The value lower than 1 meant $c_{S,Cu} < c_{T,Cu}$, suggesting that major Cu species dispersed within the pores in S-1 and Meso-1. On the contrary, the value larger than 1 indicated $c_{S,Cu} > c_{T,Cu}$, therefore justifying major Cu species dispersed on the surface of Meso-2. The $c_{S,Cu} / c_{T,Cu}$ of 2.5 wt% Cu/S-1 was the smallest among the three samples, indicating that Cu species was thoroughly dispersed in the mesoporous walls.[35] From the analysis of the mass concentration, both stability and $S_{BET}$ of the support greatly affected the distribution of the Cu species. It could be presumed that the uniformity and stability of S-1 and great $S_{BET}$ of Meso-1 could provide a relatively large distribution area for copper species. As a result, this led to a larger degree of bonding between copper species and hydroxyl-terminated silicone, promising the generation of more Cu-O-Si species.

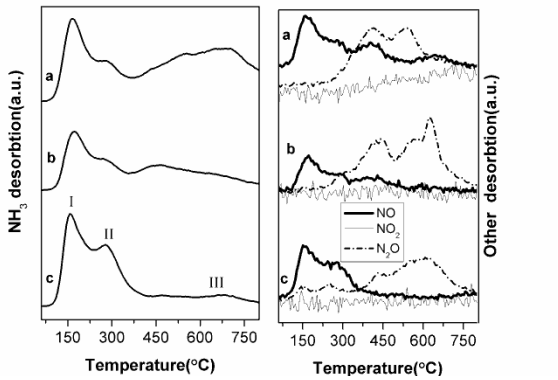


Fig. 5. The $NH_3$-TPD-MS pictures of the samples: a 2.5 wt% Cu/Meso-2; b 2.5 wt% Cu/Meso-1; c 2.5 wt% Cu/S-1.

The XPS profiles (Cu 2p) of Cu/S-1 with different Cu loading are shown in Fig. 4B. Two Cu $2p_{3/2}$ peaks (about 933.0 and 934.5 eV), attributed to dispersed CuO species and Cu-O-Si or Cu-O-Cu species, were observed.[47-49] The $c_{S,Cu} / c_{T,Cu}$ decreased from 0.25 to 0.06 with the increase of Cu loading from 0.5 to 14.0 wt%. This meant that a large amount of Cu species dispersed more easily within the pore than on surface in S-1. The appearance and increase of Cu-O-Cu species caused the dramatic decrease of Cu-O-Si species.

For the used samples containing 2.5 wt% copper, the losses of surface Cu content for S-1, Meso-1 and Meso-2 were 9%, 30% and 90%, respectively, indicating that Cu species on S-1 were the most stable among the three catalysts.

**3.1.6 $NH_3$-TPD-MS**

The $NH_3$-TPD-MS measurements were carried out to evaluate the interaction between ammonia and the catalysts containing 2.5 wt% copper, and the obtained profiles are shown in Fig. 5. On the three catalysts, the main evolved gases were $NH_3$, NO and $N_2O$ with trace $NO_2$. This could be explained by the fact that part of the chemisorbed $NH_3$ was oxidized to NO, $N_2O$ and $NO_2$ during desorption process by the catalysts. Three $NH_3$ desorption peaks at 150, 270 and 400-800 ℃ were assigned to $NH_3$ desorption on weak, medium-strong and strong acid sites, respectively, indicating that there were at least three kinds of interaction between the catalysts and $NH_3$.

The total amount of the desorbed $NH_3$ on 2.5 wt% Cu/Meso-2, 2.5 wt% Cu/Meso-1 and 2.5 wt% Cu/S-1 was 1.1, 0.9 and 1.8 mmol, respectively. The ratio of the three peaks corresponded to the reactive amounts of acid sites. The $S_a / S_b / S_c$ (peak area ratio) of $NH_3$ which desorbed from the three catalysts at 150, 270 and 400-800 ℃ were 1.0 / 0.6 / 1.2, 1.0 / 1.2 / 3.5 and 1.0 / 0.5 / 0.1, respectively. The proportion of weak and medium-strong acid sites on Cu/S-1 was the largest, while the part of strong acid sites was the lowest. In contrast, the proportion of medium-strong acid sites on Cu/Meso-2 was the lowest, while the part of strong

**Table 2.** The activity over different catalysts[a]

| Entry | Catalyst | Yield (mol %) | | | Conversion of benzene (%) | Selectivity to aniline (%) |
|---|---|---|---|---|---|---|
| | | Aniline | Phenol | DHB | | |
| 1 | S-1 | 0.0 | 1.4 | 0.1 | 2.3(1.4)[c] | 0.0 |
| 2 | Meso-1 | 0.0 | 1.2 | 2.1 | 4.1(3.3) | 0.0 |
| 3 | Meso-2 | 0.0 | 1.2 | 0.2 | 2.2(1.4) | 0.0 |
| 4 | CuO | 0.1 | 0.3 | 0.0 | 1.2(0.4) | 25.0 |
| 5 | 2.5wt%Cu/S-1 | 4.4 | 0.8 | 0.2 | 6.2(5.4) | 81.5 |
| 6 | 2.5wt%Cu/Meso-1 | 1.7 | 1.5 | 0.3 | 4.3(3.5) | 48.6 |
| 7 | 2.5wt%Cu/Meso-2 | 0.5 | 0.3 | 0.2 | 1.9(1.0) | 50.0 |
| 8[b] | 2.5wt%Cu/S-1 | 5.4 | 1.4 | 0.5 | 8.1(7.3) | 74.0 |

[a] Reaction condition: 1.0 g catalyst, 40.0 ml $H_2O$, 2.8 mmol $C_6H_6$, 133.0 mmol $NH_3·H_2O$ and 22.6 mmol $H_2O_2$, reaction temperature 60 ℃, reaction time 8 h. [b] Optimal reaction condition: 0.5 g catalyst, 40.0 ml $H_2O$, 2.8 mmol $C_6H_6$, 133.0 mmol $NH_3·H_2O$ and 18.1 mmol $H_2O_2$, reaction temperature 60 ℃, reaction time 4 h. [c] Value calculated by Moles of all products / Moles of initial benzene × 100, the difference between the two vaule indicated some losses of benzene in the process.

acid sites was the largest.

Interestingly, the desorption temperature of $NH_3$ was almost the same as that of NO gas. However, three $N_2O$ peaks were detected at 450, 580 and 650 ℃. The profile of Cu/Meso-2 possessed the largest peak area at 450 ℃ and the smallest one at 650 ℃. On the Cu/Meso-1, the area of the three peaks was almost the same. In contrast, the profile of Cu/S-1 exhibited the smallest peak area at 450 ℃ and the largest one at 650 ℃. These results indicated desorptive reaction of $NH_3$ from the catalysts, originated from different degree of activation of the N–H bond of $NH_3$ and/or different interaction of $NO_x$ formed with the catalysts.

### 3.2. Catalytic amination of benzene

The results of amination of benzene to aniline over different catalysts are shown in Table 2. No aniline was detected over the three bare supports. Aniline could be generated over copper oxide and copper doped porous silica. When 2.5 wt% Cu/S-1 was used as catalyst, the yield of aniline (4.4%) and the conversion of benzene (6.2%) was obtained with a selectivity of 81.5% (Entry 5) at 60 ℃. The main by-products detected were phenol (0.8%) and dihydroxybenzenes (DHB) (0.2%) with trace nitrobenzene. The activities of 2.5 wt% Cu/Meso-1 and Cu/Meso-2 were poor, and the yield of aniline was significantly low (1.7%, 0.5%) with low selectivity (48.6%, 50.0%). The 2.5 wt% Cu/Meso-1 was more effective to produce phenol. The lowest yield of aniline (0.1%) was obtained over CuO.

Fig. 6 illustrates the influence of Cu loading on the reaction. With the increase of Cu loading, the yield of aniline, conversion of benzene and selectivity to aniline went up initially, reached the maxima of 4.4%, 6.2% and 81.5% respectively at 2.5 wt% Cu/S-1 and then decreased. However, the yield of phenol initially decreased and then increased. The yield of DHB monotonously increased from 0.1 to 0.9% with the increase of Cu loading from 0.5 to 14.0 wt%. It was clear that excessive or inadequate copper species were more advantageous to hydroxylation of benzene. The results were in agreement with our previous reports.[19, 20] DR UV-vis (Fig. 2 and S5†) and XPS (Fig. 4) indicated the existence of Cu-O-Si species, dispersed copper species and Cu-O-Cu species on the catalysts with different Cu loading on mesoporous silica. Over S-1 support (Fig. 2 B and S5†), the relative amount

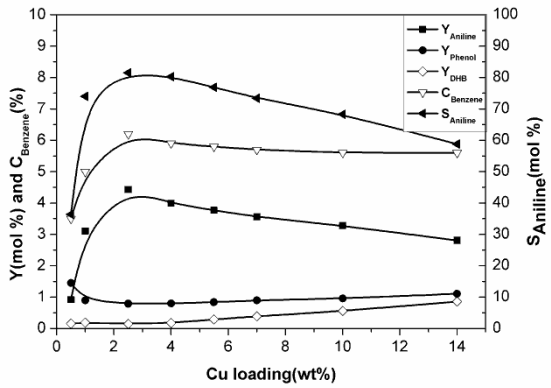


**Fig. 6.** The effect of Cu loading on the yield of products, the conversion of benzene and the selectivity to aniline. Reaction condition: 1.0 g catalyst, 40.0 ml $H_2O$, 2.8 mmol $C_6H_6$, 133.0 mmol $NH_3·H_2O$ and 22.6 mmol $H_2O_2$, reaction temperature 60 °C, reaction time 8 h.

of Cu-O-Si species initially went up, reached the maximum on 2.5 wt% Cu/S-1, and then decreased gradually with the increase of Cu loading. When the Cu loading was greater than 5.5 wt% (Fig. S5G-J†), the Cu-O-Cu species was generated and its relative amount increased obviously with the increase of Cu loading, accompanied by the decrease of Cu-O-Si species. Remarkably, with the increase of Cu loading, the catalytic activity increased obviously and then decreased gradually. The best catalytic amination performance could be obtained on 2.5 wt% Cu/S-1.

Our previous work[20] indicated that Cu-O-Ti could form by doping a certain amount of Cu on the TS-1 zeolite. Cu-O-Ti species could weaken the acidity of the initial strong acid sites and promote the chemical adsorption of $NH_3$ on Cu-TS-1, and thus promising the selective activation of the N-H bond of $NH_3$ and the oxyamination of benzene. Similar to our previous $NH_3$-TPD experiments over Cu-TS-1, four kinds of gaseous molecules ($NO_2$, $N_2O$, NO and $NH_3$) desorbed from the catalyst were also observed (Fig. 5). The result demonstrated that $NH_3$ could be adsorbed and N-H bond of $NH_3$ could be selectively activated on the copper doped catalysts. Therefore, it suggested that Cu-O-Si played similar role to Cu-O-Ti in the direct amination. That is,



 

Cu-O-Si species could also promote the chemical adsorption of $NH_3$ on $Cu/SiO_2$, and therefore promising the selective activation of the N-H bond of $NH_3$ and the oxyamination of benzene. On the catalysts containing 2.5 wt% copper, no large particles of CuO were detected by XRD (Fig. 1A) and TEM (Fig. S6†) . XPS (Fig. 4A) and ICP showed high dispersion of Cu species on S-1, which promised the bonding of Cu to the hydroxyl-terminated silicone, forming Cu–O–Si species on the framework of the catalysts. With the highest $S_{BET}$, Meso-1 could improve the dispersion of Cu species, resulting in the largest relative amount of Cu-O-Si species on 2.5 wt% Cu/Meso-1, as indicated by DR UV-vis. However, 2.5 wt% Cu/S-1 performed better than 2.5 wt% Cu/Meso-1. The result indicated that Cu-O-Si species on catalysts was not the unique important factor affecting the catalytic performance.

Previous work reported that medium-strong acid sites on catalysts could be important for amination.[20] Compared to the other two catalysts, 2.5 wt% Cu/S-1 possessed more amounts of medium-strong acid sites which provided enough sites for the effective chemical adsorption of $NH_3$, and more Cu-O-Si species which provided enough active sites for the activation of N-H bond of the $NH_3$. When 2.5 wt% Cu/Meso-2 was employed as catalyst, it could not provide enough sites for the effective chemical adsorption of $NH_3$ nor active sites for the activation of N-H bond of $NH_3$. Though 2.5 wt% Cu/Meso-1 could provide most active sites for $NH_3$ activation, there were not enough sites for the effective chemical adsorption of $NH_3$. The outstanding catalytic amination performance was obtained due to the existence of more amounts of both medium-strong acid sites and Cu-O-Si species on 2.5 wt% Cu/S-1. The results indicated that Cu-O-Si species in $Cu/SiO_2$ played almost the same role as Cu-O-Ti species over Cu/TS-1 in amination. On the other hand, the adsorption of $NH_3$ on medium-strong acid sites also played important role in the total reaction.

In present work, the formation of aniline, as well as phenol and DHB over all catalysts, showed that C-H bond of benzene could be activated in the presence of $H_2O_2$ under mild conditions. Although the conversion of benzene (1.2%) (Table 2, Entry 4) could be obtained over CuO, the catalytic activity of CuO was inferior to copper doped catalyst. S-1 turned out to be the best support for the activation of C-H bond of benzene (Table 2, Entry 5). Remarkably, with the increase of Cu loading, the conversion of benzene went up initially, reached the maxima of 6.2% on 2.5 wt% Cu/S-1 (Fig. 6) and then decreased. The results conformed to our previous work[19, 20], that is, C-H bond of benzene could be effectively activated over Cu/S-1 under the present reaction condition. The formation of aniline was dependent on both the selective activation of N-H bond of $NH_3$ and C-H bond of benzene on $Cu/SiO_2$.

The effect of other reaction conditions on amination of benzene to aniline have been investigated (S3†). Under the optimized conditions, the highest yield of aniline (5.4%) and selectivity of aniline (74.0%) was obtained over Cu/S-1 (Table 2, Entry 8). The results showed that there was a competition between amination and hydroxylation of benzene in the reaction system.[19,50] It was revealed that a diluted instantaneous concentration of both ammonia and $H_2O_2$ was favourable to amination.

**Table 3** The results of catalytic amination of substituted benzenes

| Substrate | Products yield on the aromatic ring (mol %) | | Other | Selectivity to aminated products (%) |
|---|---|---|---|---|
| | Amination | hydroxylation | | |
| nitrobenzene | 0.2 | n.d | - | 100.0 |
| chlorobenzene | 4.8 | 0.2 | - | 96.0 |
| benzene | 5.4 | 1.9 | - | 74.0 |
| toluene | 4.3 | 3.1 | 1.5 | 48.3 |
| anisole | 7.4 | 4.3 | - | 63.2 |
| phenol | n.d | 3.5 | n.d | - |
| paraxylene | 1.2 | 1.5 | 1.6 | 27.9 |
| mesitylene | 0.4 | 0.3 | 1.1 | 22.2 |

Reaction condition: 0.5 g catalyst, 40.0 ml $H_2O$, 2.8 mmol substituted benzenes, 133.0 mmol $NH_3·H_2O$ and 18.1 mmol $H_2O_2$, reaction time 4 h, reaction temperature 60 ℃.

To further investigate the catalytic activity of the Cu/S-1 in the direct amination of benzene, 2.5 wt% Cu/S-1 was operated under the optimized conditions using kettle-type[20] and RD reactor[19] (S4†). The result showed that 2.5 wt% Cu/S-1 possessed comparable catalytic activity as 2.5 wt% Cu/h-TS-1, confirming that Cu/S-1 could play almost the same role as Cu/h-TS-1 in the direct amination of benzene. However, the catalytic activity of Cu-O-Ti would be better than that of Cu-O-Si.

In addition, the possible reaction pathway of ammination for aniline formation was investigated (S5†). The experimental results showed that hydroxylamine was the possible intermediate, which agreed well with the previous report.[19]

### 3.3 The stability and recyclability of the catalyst

The stability of Cu/S-1 (Table S1†) was measured as well. The selectivity to aniline and catalytic activity decreased after the first two runs. In the next three recycles, the catalytic performance was almost unchanged, suggesting a good recyclability of the catalyst.

The used Cu/S-1 was further investigated by XRD (Fig. S1†), BET (Table 1 and Fig. S3†) and TEM (Fig. S6†). The results showed that the used Cu/S-1 still possessed mesoporous and MFI crystal structure remained after being used. ICP results in Table S1† indicated that the Cu loading of the catalyst decreased slightly from 2.48 to 2.13% after being used in the first two runs and then kept almost unchanged with further runs. These results demonstrated the good stability of the Cu/S-1.

### 3.4. Catalytic amination of substituted benzenes

Under the optimized conditions, the amination was extended to substituted benzenes. The results are listed in Table 3. Amination products could be detected for all substituted benzenes except phenol. When anisole was used as substrate, the highest yields of amination (7.4%) and hydroxylation (4.3%) products on the aromatic ring were obtained with a selectivity of 63.2% to arylamine. For chlorobenzene, the high yield (4.8%) and selectivity (96.0%) to arylamine were obtained. Although the selectivity reached the maximum of 100.0%, the yield of amination products of nitrobenzene was the lowest (0.2%). The results showed that Cu/S-1 catalyst could effectively activate the C-H bond on aromatic ring of substituted benzenes and N-H bond of ammonia in the presence of $H_2O_2$.

Among these substrates, the electron donating property of substituent followed the order: -OH >-$OCH_3$ > -$CH_3$> -Cl > -$NO_2$.

With the increase of the ability of the electron donation, the yield of the amination products increased from 0.2% to 7.4% for -$OCH_3$. However, no amination products were detected when phenol was used as substrate. It might be that the amination products were unable to desorb from catalyst surface and further inhibited their formation.[18] Because the substituent of toluene, paraxylene and mesitylene involved into the reaction, the selectivity of their amination products was low (22.2-48.3%). With the increase of the number of substituent, the yield of products on the aromatic ring obviously decreased due to the steric hindrance of the substituent. It was worth noting that ortho-isomers were preferentially produced from substituted benzenes (Table S2†). These results confirmed that the reaction possessed possibly electrophilic characters.

The literature[51] and our previous[5] work reported that the active species were the electrophilic ammonia radical cation ($\bullet NH_3^+$) when hydroxylamine was used as aminating agent. We found that hydroxylamine could be generated in present reaction system. The results suggested that $\bullet NH_3^+$ was the possible active species and hydroxylamine was the reaction intermediate in this reaction. More studies on reaction mechanism would be conducted in future work.

## 4 Conclusions

Copper doped S-1 was effective in the direct aromatic ring amination of benzene and substituted benzenes with $NH_3$·$H_2O$ and $H_2O_2$. The MFI structure of S-1 with hydroxyl-terminated silicone was found to facilitate the formation of Cu-O-Si species. This Cu-O-Si species was identified to be one of the important factors responsible for the generation of aniline. Besides, the medium-strong acid sites were also determined as a vital factor for the amination process. Because 2.5 wt% Cu/S-1 possessed more amounts of Cu-O-Si species and medium-strong acid sites, it exhibited the best catalytic performance in the reaction. Over 2.5 wt% Cu/S-1, the amination process could provide 5.4% aniline yield in a close system at 60 ℃, while a yield of 10.8% was obtained using RD reactor. The concentration of reactants was another crucial factor to the reaction, and a diluted instantaneous concentration of both ammonia and $H_2O_2$ was favourable to amination.

## Acknowledgements

Financial support from the NSFC (No. 21172157, No. 21372167 and No. 201321061) of China, and technical support by Analytic and Testing Centre of Sichuan University are cordially acknowledged. The suggestions by the reviewers were highly appricated.

## Notes and references

[a] *Key Laboratory of Green Chemistry and Technology, Ministry of Education, College of Chemistry, Sichuan University, 29 Wangjiang Road, Chengdu, Sichuan, 610064, China. Fax: +86-28-85411105. Tel: +86-28-85411105. E-mail address: changweihu@scu.edu.cn or gchem@scu.edu.cn.*

[b] *School of life sciences ,Guizhou Normal University, 116 Baoshan North Road, Guiyang 550001, China*

† Electronic Supplementary Information (ESI) available: [Supplemental figures, texts and tables]. See DOI: 10.1039/b000000x/

1. Q. Shen and J. F. Hartwig, *J. Am. Chem. Soc.*, 2006, **128**, 10028.
2. D. S. Surry and S. L. Buchwald, *J. Am. Chem. Soc.*, 2007, **129**, 10354.
3. H. Xu and C. Wolf, *Chem. Commun.*, 2009, 3035.
4. H. Yuzawa and H. Yoshida, *Chem. Commun.*, 2010, **46**, 8854.
5. L. Zhu, B. Guo, D. Tang, X. Hu, G. Li and C. Hu, *J. Catal.*, 2007, **245**, 446.
6. A. Hagemeyer, R. Borade, P. Desrosiers, S. Guan, D. M. Lowe, D. M. Poojary, H. Turner, H. Weinberg, X. Zhou, R. Armbrust, G. Fengler and U. Notheis, *Appl. Catal. A: Gen.*, 2002, **227**, 43.
7. S. Singha and K. M. Parida, *Catal. Sci. Technol.*, 2011, **1**, 1496.
8. K. M. Parida, D. Rath and S. S. Dash, *J. Mol. Catal. A: Chem.*, 2010, **318**, 85.
9. K. M. Parida, S. S. Dash and S. Singha, *Appl. Catal. A: Gen.*, 2008, **351**, 59.
10. J. P. Wibaut, *Berichte*, 1917, **50**, 541.
11. N. Hoffmann and M. Muhler, *Catal. Lett.*, 2005, **103**, 155.
12. N. Hoffmann, E. Loffler, N. A. Breuer and M. Muhler, *ChemSusChem*, 2008, **1**, 393.
13. J. T. Anders, *US Pat.*, 2009/0292144, 2009.
14. P. Desrosiers, S. Guan, A. Hagemeyer, D. M. Lowe, C. Lugmair, D. M. Poojary, H. Turner, H. Weinberg, X. Zhou, R. Armbrust, G. Fengler and U. Notheis, *Catal. Today*, 2003, **81**, 319.
15. F. V. Laar, *US Pat.*, 2009/0203941, 2009.
16. J. u. Becker and W. F. H ̈olderich, *Catal. Lett.*, 1998, **54**, 125.
17. S. A. Axon, WO Pat., 99/10 311, 1999.
18. H. Yuzawa, J. Kumagai and H. Yoshida, *J. Phys. Chem. C*, 2013, **117**, 11047.
19. T. Yu, Q. Zhang, S. Xia, G. Li and C. Hu, *Catal. Sci. Technol.*, 2014, **4**, 639.
20. B. Guo, Q. Zhang, G. Li, J. Yao and C. Hu, *Green Chem.*, 2012, **14**, 1880.
21. C. Hu, L. Zhu and Y. Xia, *Ind. Eng. Chem. Res.*, 2007, **46**, 3443.
22. F. Zaccheria, R. Psaro and N. Ravasio, *Green Chem.*, 2009, **11**, 462.
23. A. Cooper, B. Bachiller-Baeza, J. A. Anderson, I. Rodriguez-Ramos and A. Guerrero-Ruiz, *Catal. Sci. Technol.*, 2014, **4**, 1446.
24. L. Xie, F. Liu, K. Liu, X. Shi and H. He, *Catal. Sci. Technol.*, 2014, **4**,1104.
25. J. Lin, X. Zhao, Y. Cui, H. Zhang and D. Liao, *Chem. Commun.*, 2012, **48**, 1177.
26. N. Xia and M. Taillefer, *Angew. Chem., Int. Ed.*, 2009, **48**, 337.
27. J. Kim and S. Chang, *Chem. Commun.*, 2008, 3052.
28. E. M. Flanigen, J. Bennett, R. Grose, J. Cohen, R. Patton and R. Kirchner, *Nature*, 1978, **271**, 512.
29. H. Wang, L. Liang, W. Zhang and J. Han, *J. Porous Mater.*, 2012, **19**, 889.
30. C. Wen, A. Yin, Y. Cui, X. Yang, W.-L. Dai and K. Fan, *Appl. Catal. A: Gen.*, 2013, **458**, 82.
31. Q. Hu, B. J. Dou, H. Tian, J. J. Li, P. Li and Z. P. Hao, *Micropor. Mesopor. Mater.*, 2010, **129**, 30.
32. R. Wang, X. Guo, X. Wang, J. Hao, G. Li and J. Xiu, *Appl. Catal. A: Gen.*, 2004, **261**, 7.
33. K. Sing, D. Everett, R. Haul, L. Moscou, R. Pierotti, J. Rouquerol and T. Siemieniewska, *Pure Appl. Chem.*, 1985, **57**, 603.
34. A. Patel, P. Shukla, T. Rufford, S. Wang, J. Chen, V. Rudolph and Z. Zhu, *Appl. Catal. A: Gen.*, 2011, **409**, 55.
35. E. S. Vasiliadou and A. A. Lemonidou, *Appl. Catal. A: Gen.*, 2011, **396**, 177.
36. K. V. Chary, G. V. Sagar, C. S. Srikanth and V. V. Rao, *J. Phys. Chem. B*, 2007, **111**, 543.
37. P. J. Smeets, M. H. Groothaert and R. A. Schoonheydt, *Catal. Today*, 2005, **110**, 303.
38. Z. Sun, C. Bai, S. Zheng, X. Yang and R. L. Frost, *Appl. Catal. A: Gen.*, 2013, **458**, 103.
39. P. M. C. Zapata, M. L. Parentis, E. E. Gonzo and N. A. Bonini, *Appl. Catal. A: Gen.*, 2013, **457**, 26.
40. M. V. Konduru and S. S. Chuang, *J. Catal.*, 1999, **187**, 436.
41. J. Andas, F. Adam and I. A. Rahman, *Appl. Surf. Sci.*, 2013, **284**, 503.
42. D. V. Vu, M. Miyamoto, N. Nishiyama, S. Ichikawa, Y. Egashira and K. Ueyama, *Micropor. Mesopor. Mater.*, 2008, **115**, 106.
43. S. Zhao, H. Yue, Y. Zhao, B. Wang, Y. Geng, J. Lv, S. Wang, J. Gong and X. Ma, *J. Catal.*, 2013, **297**, 142.

44. L.-F. Chen, P.-J. Guo, M.-H. Qiao, S.-R. Yan, H.-X. Li, W. Shen, H.-L. Xu and K.-N. Fan, *J. Catal.*, 2008, **257**, 172.
45. J. Gong, H. Yue, Y. Zhao, S. Zhao, L. Zhao, J. Lv, S. Wang and X. Ma, *J. Am. Chem. Soc.*, 2012, **134**, 13922.
46. A. Gervasini, M. Manzoli, G. Martra, A. Ponti, N. Ravasio, L. Sordelli and F. Zaccheria, *J. Phys. Chem. B*, 2006, **110**, 7851.
47. Z. He, H. Lin, P. He and Y. Yuan, *J. Catal.*, 2011, **277**, 54.
48. S. Zhu, X. Gao, Y. Zhu, Y. Zhu, H. Zheng and Y. Li, *J. Catal.*, 2013, **303**, 70.
49. S. Natesakhawat, J. W. Lekse, J. P. Baltrus, P. R. Ohodnicki, B. H. Howard, X. Deng and C. Matranga, *ACS Catal.*, 2012, **2**, 1667-1676.
50. F. Xiao, *J. Catal.*, 2001, **199**, 273.
51. N. I. Kuznetsova, L. I. Kuznetsova, L. G. Detusheva, G. P. Pez and H. Cheng, *J. Mol. Catal. A: Chem.*, 2000, **161**, 1.